Pseudo-Elasticity at Large Strains in Au Nanocrystals

X. Wendy Gu[1,2*], Lindsey A. Hanson[1,3*], Carissa N. Eisler[4], Matthew A. Koc[1], A. Paul Alivisatos[1,4,5,6]

[1]Department of Chemistry, University of California, Berkeley, Berkeley, CA 94720, USA

[2]Department of Mechanical Engineering, Stanford University, Stanford, CA 94305, USA

[3]Department of Chemistry, Trinity College, Hartford, CT 06106, USA

[4]Materials Science Division, Lawrence Berkeley National Laboratory, Berkeley, CA 94720, USA

[5]Department of Materials Science and Engineering, University of California, Berkeley, Berkeley, CA 94720, USA

[6]Kavli Energy NanoScience Institute, University of California, Berkeley and Lawrence Berkeley National Laboratory, Berkeley, CA 94720, USA

* These authors contributed equally to this work

Corresponding author:

A. Paul Alivisatos

D43 Hildebrand Hall, University of California, Berkeley 94720

510-643-2050

paul.alivisatos@berkeley.edu

Keywords: plasticity, size effects, absorbance, plasmonics, high pressure

Abstract

Pseudoelasticity in metals is typically associated with phase transformations (e.g. shape memory alloys) but has recently been observed in sub-10 nm Ag nanocrystals that rapidly recovered their original shape after deformation to large strains. The discovery of pseudoelasticity in nanoscale metals dramatically changes the current understanding of the properties of solids at the smallest length scales, and the motion of atoms at surfaces. Yet, it remains unclear whether pseudoelasticity exists in different metals and nanocrystal sizes. The challenge of observing deformation at atomistic to nanometer length scales has prevented a clear mechanistic understanding of nanoscale pseudoelasticity, although surface diffusion and dislocation-mediated processes have been proposed. We further the understanding of pseudoelasticity in nanoscale metals by using a diamond anvil cell to compress colloidal Au nanocrystals under hydrostatic and non-hydrostatic pressure conditions. Nanocrystal structural changes are measured using optical spectroscopy and transmission electron microscopy, and modeled using electrodynamic theory. We find that 3.9 nm Au nanocrystals exhibit pseudoelastic shape recovery after deformation to large uniaxial strains of up to 20%, which is equivalent to an ellipsoid with an aspect ratio of 2. Nanocrystal absorbance efficiency does not recover after deformation, which indicates that

crystalline defects may be trapped in the nanocrystals after deformation.

Main text

Pseudoelasticity describes the reversible deformation of a material that is strained past its elastic limit, through a process in which atomic bonds are broken and reformed. Recently, rapid pseudoelastic recovery from large strains was observed in sub-10 nm Ag nanoparticles inside of a transmission electron microscope (TEM). [1] The surprising observation of pseudoelasticity in Ag nanoparticles is diametrically opposed to the classical behavior of metals, in which irreversible plastic deformation occurs at large strains. This discovery adds to the growing body of evidence that strength, deformation and defect dynamics in nanoscale solids cannot be extrapolated from the properties of their bulk counterparts. Pseudoelastic metallic nanostructures should have superior performance, including shape memory at low temperatures and the ability to rapidly heal from applied stresses. Pseudoelasticity in metal nanocrystals has been attributed to rapid surface diffusion, [1,2] but defect mediated processes such as the escape of dislocations through free surfaces,[13,14] and the reversible passage of twin boundaries [5,6] are other possible mechanisms. Further insight into this phenomenon requires investigation of other nanocrystal sizes and metals at realistic

temperatures and time scales, which can be challenging to achieve *in-situ* TEM or through atomistic modeling.

Here, 3.9 nm Au nanocrystals are compressed inside of a diamond anvil cell to determine whether deformation is reversible under volumetric and deviatoric strains. The outstanding physical properties of Au nanocrystals have enabled their widespread use in photonics, [7,8] catalysis, [9,10] sensing [11,12] and biomedical therapies. [13,14] The structural stability of Au nanocrystals is of interest for size and shape control during synthesis and fabrication, [15,16] and the reliable operation of nanocrystal-based devices. Pseudoelasticity is expected in 3.9 nm nanocrystals according to the surface diffusion-based mechanism developed for Ag. [1] It is unclear whether pseudoelasticity will be observed in Au, which has slower atomic surface diffusion than Ag. [17]

Diamond anvil cell compression has previously been used to study elastic properties and phase transformations in inorganic nanocrystals. [18–23] Nanocrystal structural changes are monitored *in-situ* using optical absorption spectroscopy. Absorption spectroscopy reveals the localized surface plasmon resonance of the Au nanocrystals, which is generated by the resonant oscillation of conduction electrons in response to light. The energy and intensity of the surface plasmon is highly sensitive to nanocrystal size and shape, [24–26] and can therefore be used to track deformation under

pressure. The surface plasmon also depends on the density of crystalline defects in the nanocrystal, [27,28] which is indicative of microstructural changes in the nanocrystals. We demonstrate the sensitivity of this detection method by using electrodynamics theory to model the optical response to shape and microstructural changes in the Au nanocrystals. It is found that sub-nanometer changes in nanocrystal aspect ratio lead to greater than 20 nm shifts in plasmon energy. Results from optical spectroscopy are corroborated using TEM. Using these techniques, we determine that Au nanocrystals rapidly recover their original shape after uniaxial deformation to large strains after single and multicycle loading inside of the diamond anvil cell. We believe that crystalline defects in the interior of the nanocrystal play a role in the pseudoelastic deformation based on an irreversible reduction in absorbance efficiency after pressurization.

Dodecanethiol-capped Au nanocrystals with diameters of 3.9 ± 0.9 nm were synthesized using organic-phase air-free techniques (Figure 1A). [29] Nanocrystals were transferred to the desired pressure medium, and loaded into the diamond anvil cell for cyclic pressure testing. Ethylcyclohexane was used as a hydrostatic pressure medium, and toluene was used as a non-hydrostatic pressure medium. [19,30] Nanocrystal solutions were maintained in the dilute limit to ensure that optical changes are not due to particle-particle coupling. The refractive index of ethylcyclohexane increases by less than 0.006 RIU per GPa,

while the refractive index of toluene and dodecanethiol (ligand shell) increases by 0.02 RIU per GPa (see Supporting Information). Changes in path length and concentration during pressurization are accounted for by monitoring the cross-sectional area and height of the diamond anvil cell chamber (see Supporting Information).

Figure 1B shows the extinction spectra of the Au nanocrystals under hydrostatic pressure up to 21 GPa. Extinction is dominated by absorption in nanocrystals that are much smaller than the wavelength of light, [26] so extinction is referred to as absorbance from here on out. The absorbance spectra change minimally under hydrostatic pressure. The plasmon peak wavelength (λ_{max}) increases by 5 nm as pressure is increased to 21 GPa (the spectral resolution is 2.7 nm), and returns to the original plasmon wavelength as pressure is decreased to ambient conditions. The absorbance efficiency at the plasmon wavelength per volume of solution (Q_{max}) is determined at each pressure. The change in Q_{max} from the first to the maximum pressure is within the measurement resolution, as is the change from the first to the last pressure (ambient pressure). Figure 1C shows the optical spectra of the Au nanocrystals under non-hydrostatic pressure up to 19 GPa. In contrast to the hydrostatic case, λ_{max} undergoes a large redshift as pressure is increased to 19 GPa, and then returns to its original value after the pressure is removed. The shape of the optical spectrum

at the end of the pressure cycle (ambient pressure) is similar to the initial spectrum, but Q_{max} is reduced at the end of the pressure cycle.

The changes in plasmon peak wavelength and absorbance efficiency under non-hydrostatic pressure are quantified in Figure 2 for four experiments. Maximum pressures of 15 to 24 GPa were reached in these experiments, which resulted in a redshift in λ_{max} of 46 to 68 nm (Figure 2A-D). The average optical shift is 3.2 nm/GPa. Upon removing the pressure, the final λ_{max} returned to within 0 to 8 nm of the initial λ_{max}. λ_{max} initially shifts rapidly at pressures below 3 GPa and then shifts more slowly at higher pressures (Figure 2A-D). The corresponding changes in Q_{max} are shown in Figure 2E-H. The final absorbance efficiency is 30% to 60% of the initial absorbance efficiency. The changes in Q_{max} with pressure vary across the four experiments (Figure 2E-H). In Figure 2E, Q_{max} is higher at elevated pressures. Figure 2F and H show an initial increase in Q_{max} at the first pressurized data point, and then a decrease in Q_{max} below the initial absorbance efficiency for subsequent pressures. Figure 2G shows an immediate decrease in Q_{max} with pressurization, and a Q_{max} that is lower than the initial Q_{max} for subsequent pressures. All experiments show hysteresis in Q_{max} between increasing and decreasing pressure.

The variation in the optical response across these experiments can be linked to differences in the magnitude of deviatoric pressure between experiments, and during the course of an experiment. The

deviatoric strain across the sample chamber has been quantified by measuring the change in cross-sectional area, and distance between the diamond platens for the experiments in Figure 2, and is observed to vary significantly between experiments (see Supporting Information). Previous diamond anvil cell experiments on metallic powders under non-hydrostatic pressures have shown that uniaxial stress increases linearly with average pressure; [31–33] this is likely to occur during the experiments presented here as well.

Spherical Au nanocrystals will become elongated spheroids under non-hydrostatic pressure. This change in nanocrystal shape is predicted to lead to a redshift in λ_{max}, [24–26] which agrees well with our experimental observations. The reversibility of the observed redshift indicates that the nanocrystals return to their original shape when pressure is removed, which is quite surprising considering the large pressures involved. Further evidence of nanocrystal shape recovery is provided by post-deformation TEM images of the nanocrystals (Figure 3). Nanocrystals were recovered after diamond anvil cell testing, and dispersed onto a TEM grid. Post-deformation nanocrystals are very similar in appearance to as-synthesized nanocrystals: nanocrystals are spherical and contain crystalline domains after deformation (see Supporting Information), and are able to form close-packed three-dimensional assemblies upon slow drying (Figure 3B). Ordered nanocrystal assemblies can only form from highly

monodisperse nanocrystals, [34,35] which indicates that a large fraction of nanocrystals are spherical and reasonably monodisperse after deformation. These results do not explain the reduction in Q_{max} that results from the pressure cycle, which may be due to additional microstructural changes, like the creation of crystalline defects such as dislocations.

The source of the observed changes in λ_{max} and Q_{max} under pressure is investigated using optical modeling. A finite difference time domain model was used to calculate absorption of Au nanocrystals of different sizes and shapes, without accounting for compressional effects (e.g. changes in lattice parameter, electron density or density of states). The size of the simulated nanocrystal was varied to explore the effect of volumetric strain on the optical response of Au nanocrystals under hydrostatic pressure (Figure 4a). Changes in refractive index during compression were accounted for in simulation. In agreement with the experimental observations, the simulated absorbance spectra do not change significantly when nanocrystal diameter is changed from 3.9 to 3.5 nm. The diameter of the Au nanocrystals is expected to change by this amount in experiment according to the bulk modulus for a macroscale Au structure [36] although the bulk modulus may be different for a Au nanocrystal. [20] These results indicate that compressional effects, such as changes in bound and free electron density under pressure, are not significant in

small Au nanocrystals. The effect of changing electron density is small because free electrons are delocalized outside of the nanocrystal (electron spillout effect) in nanocrystals with diameters of less than 10 nm and are not strongly affected by lattice contraction. [26,37,38] A previous simulation study observed a redshift of more than 100 nm in 10-100 nm Au nanocrystals under 5% volumetric compression when electron density effects are prominent. [37]

The simulated and experimental spectra for Au nanocrystals under hydrostatic pressure indicate that a small change in volume has a negligible effect on Au plasmonic properties. Therefore, the effect of volumetric strain can be omitted in regard to the large changes in λ_{max} and Q_{max} under non-hydrostatic pressure, although a small amount of volumetric strain occurs in these tests. The optical spectra of oblate spheroids are simulated to quantify the effects of deviatoric strain on Au nanocrystals under non-hydrostatic pressure (Figure 4B). Figure 4b shows the absorbance spectra of spheroidal Au nanocrystals with aspect ratios of 1 to 2.7 (aspect ratio is defined as the ratio of the major axis to minor axis of the ellipsoidal cross-section of the spheroid), and volume equal to a 3.9 nm sphere. λ_{max} increases from 505 nm to 600 nm when aspect ratio is increased from 1 to 2.7 (Figure 4C). Q_{max} increases to 1.12 a.u. when aspect ratio is increased to 1.2, due to the changing refractive index environment. Q_{max} decreases with further increases in aspect ratio (Figure 4D). These results support the

conclusion that the experimentally observed redshift under non-hydrostatic pressure is due to nanocrystal shape change.

While the initial increase and subsequent decrease in the simulated Q_{max} is similar to experiment (Figure 2E, F, H), the magnitude of the decrease in Q_{max} is larger in experiment than simulation. In particular, the large decrease in the experimental Q_{max} that occurs upon decreasing pressure to ambient conditions does not match the simulated change in Q_{max}, and cannot be attributed to changes in nanocrystal geometry. Previous experiments show that polycrystalline Au and Ag nanocrystals have lower absorbance efficiency (Q_{max}) than single crystalline nanocrystals, but similar plasmon wavelength (λ_{max}). [27,28] In contrast, electrodynamics simulations on crystalline defects in Au nanoshells determined that defects have no influence on optical absorbance, [39] while atomistic simulations on Ag nanocubes observed a significant redshift and reduction in absorbance efficiency in sub-3 nm nanocrystals containing planar defects (e.g. partial and full dislocations). [40] These conflicting reports indicate that further studies are needed to understand the effect of defects on noble nanocrystal plasmonic properties. The presence of crystalline defects is modeled in our simulation as an increase in free electron damping (see Supporting Information). The density of crystalline defects is increased until equivalent to a Au thin film with a 1.2 nm grain size. [41] This leads to a 10 nm redshift and a 33% decrease in absorbance efficiency.

This result indicates that the experimentally observed changes in λ_{max} and Q_{max} are due to a combination of shape change and the emergence of defects in the Au nanocrystals under pressure.

Using these simulation results, we estimate that the Au nanocrystals experience uniaxial strain of up to 14-20% in the non-hydrostatic experiments assuming that the Au nanocrystals become oblate spheroids under pressure with aspect ratios of 1.6 to 2. This strain far exceeds the elastic limit for bulk Au. Previous diamond anvil cell experiments on Au and other metals in non-hydrostatic environments show that yield strength increases by ~1 GPa over the pressure range in our experiments. [32,33,42] The uniaxial pressure in our experiments exceeds the pressure-dependent yield stress for Au such that plastic deformation (breaking of atomic bonds) is expected to occur in the Au nanocrystals. The reversible deformation observed in the Au nanocrystals involves a pseudoelastic transformation in which the Au nanocrystals recover their original shape after atoms within the nanocrystals lose their original coordinates and connectivity. This agrees with the recent observation of pseudoelasticity in sub-10nm Ag nanocrystals, [1] but is the first time this phenomenon has been observed in an ensemble of nanocrystals, and outside of an electron microscope. Previous diamond anvil cell experiments on ~40 nm colloidal Au nanocrystals at dilute concentrations under non-hydrostatic conditions resulted in irreversible deformation and fracture

under pressure. [21,22] Thus, pseudoelasticity is active on experimental time scales (minutes) only in very small Au nanocrystals.

No dislocations were observed during the pseudoelastic deformation of sub-10 nm Ag nanocrystals, [1] although there may be dislocations that are invisible at the imaging conditions, or that move too rapidly to be captured by TEM. In contrast, our optical measurements and modeling indicate that crystalline defects form in the interior of the Au nanocrystals during deformation. The mechanism behind the pseudoelasticity in the Au nanocrystals is investigated by compressing nanocrystal samples over two pressure cycles to determine the time and history dependence of the optical response. Figure 5A and C correspond to an experiment in which pressure cycle 2 occurred thirty minutes after the end of cycle 1. The change in λ_{max} is extremely similar over the two pressure cycles (Figure 5A). The final λ_{max} is identical to the initial λ_{max} after cycle 1, and is redshifted by 10 nm relative to the initial λ_{max} after cycle 2. The shape of the Q_{max} vs. pressure curve is similar for the two cycles (Figure 3C), but the initial absorbance efficiency of cycle 2 is reduced by 0.45 relative to cycle 1. The shape of the Q_{max} vs. pressure curve is similar for the two cycles because the change in strain of the diamond anvil cell chamber is very similar for the two cycles (see Supporting Information). In the experiment in Figure 3B and D, cycle 2 occurs 15.5 hours after cycle 1. Interestingly, the initial Q_{max} at the beginning of the second cycle is

significantly greater than the final Q_{max} of the first cycle (Figure 3D), which indicates that there is recovery of absorbance efficiency in this time.

In the experiments shown in Figure 5, final Q_{max} is always lower than the initial Q_{max} within one pressure cycle. This indicates that structural deformation accumulates during the course of the pressure cycle, and can be retained between pressure cycles. The time dependent changes in Q_{max} between pressure cycles presents an intriguing clue as to the structural changes occurring in the nanocrystals, but require more careful investigation before conclusions can be made. The post-deformation TEM images of nanocrystals were taken several days after the diamond anvil cell experiments were performed (Figure 3). Crystalline defects that were initially present in the nanocrystals after deformation may have healed before imaging through dislocation-mediated processes such as escape through free surfaces. [3,4] Direct structural measurements, such as through high-pressure X-ray diffraction, could provide further insights into the mechanism of pseudoelasticity in Au nanocrystals.

In summary, 3.9 nm Au nanocrystals are compressed under hydrostatic and non-hydrostatic conditions in a diamond anvil cell. Changes in nanocrystal structure under pressure are monitored using optical absorbance. Nanocrystals under hydrostatic pressure do not exhibit a change in plasmon wavelength. Nanocrystals under non-

hydrostatic pressure exhibit a reversible redshift of the plasmon wavelength of up to 68 nm over ~20 GPa. The absorbance efficiency is reduced to 30-60% of its original value after the non-hydrostatic pressure cycle. Optical modeling was performed to correlate changes in absorbance to strain and lattice disorder in the nanocrystals. The results of this model indicate that the nanocrystals deform up to ~20% strain (equivalent to an aspect ratio of 2) under non-hydrostatic pressure, yet are able to recover their original spherical shape. Post-compression TEM images demonstrate that the nanocrystals return to their original shape after the pressure cycle. The Au nanocrystals exhibit room temperature pseudoelastic shape recovery at large strains, which differs completely from bulk scale behavior. A reduction in nanocrystal absorbance efficiency is related to increased free electron scattering due to the presence of crystalline defects. This indicates that the non-hydrostatic deformation of Au nanocrystals likely leads to an increase in the number of defects such as dislocations in the nanocrystals.

Our discovery of pseudoelasticity in small Au nanocrystals implies that the metallic nanostructures used in nanoscale machines, devices and patterned surfaces may demonstrate rapid self-healing and resilience against external stresses and strains. The relevance of these findings extends beyond nanofabrication and crystal growth. Au nanocrystals could be used as nanoscale strain gauges that can

differentiate between volumetric and deviatoric strains with a reversible, pressure-dependent optical readout that has better sensitivity than existing nanocrystal sensors. [19,23,43–45] These attributes of Au nanocrystals could be used to measure biological forces, which are of great importance in isolated and collective cell behavior. Our results also present the possibility of pseudoelastic deformation in nano-precipitates in bulk metallic alloys. It remains to be seen whether pseudoelasticity is universal across different nanoscale metals, and when embedded in a variety of matrices.

Acknowledgements

We gratefully acknowledge financial support from the U.S. Department of Energy, Office of Science, Office of Basic Energy Sciences, Materials Sciences and Engineering Division, under contract number DE-AC02-05CH11231 within the Inorganic/Organic Nanocomposites Program (KC3104). C. N. Eisler acknowledges support from the Office of Energy Efficiency & Renewable Energy Postdoctoral Fellowship Program (U.S. Department of Energy). We would like to thank Dr. Son Nguyen for help with synthesizing nanocrystals, and Prof. Bill Nix, Andy Minor and Raymond Jeanloz for a critical reading of the manuscript.

References

[1] J. Sun, L. He, Y.-C. Lo, T. Xu, H. Bi, L. Sun, Z. Zhang, S. X. Mao, and J. Li, Nat. Mater. **13**, 1007 (2014).

[2] O. Kovalenko, C. Brandl, L. Klinger, and E. Rabkin, Adv. Sci. **4**, 1700159 (2017).

[3] D. Mordehai, E. Rabkin, and D. J. Srolovitz, Phys. Rev. Lett. **107**, 96101 (2011).

[4] R. Kositski and D. Mordehai, Acta Mater. **136**, 190 (2017).

[5] W. Liang, M. Zhou, and F. Ke, Nano Lett. **5**, 2039 (2005).

[6] J. Wang, Z. Zeng, C. R. Weinberger, Z. Zhang, T. Zhu, and S. X. Mao, Nat. Mater. **14**, 594 (2015).

[7] W. L. Barnes, A. Dereux, and T. W. Ebbesen, Nature **424**, 824 (2003).

[8] S. Lal, S. Link, and N. J. Halas, Nat. Photonics **1**, 641 (2007).

[9] P. V. Kamat, J. Phys. Chem. B **106**, 7729 (2002).

[10] J. Zeng, Q. Zhang, J. Chen, and Y. Xia, Nano Lett. **10**, 30 (2010).

[11] C. Sönnichsen, B. M. Reinhard, J. Liphardt, and A. P. Alivisatos, Nat. Biotechnol. **23**, 741 (2005).

[12] K. A. Willets and R. P. Van Duyne, Annu. Rev. Phys. Chem. **58**, 267 (2007).

[13] X. Huang, I. H. El-Sayed, W. Qian, and M. A. El-Sayed, J. Am. Chem. Soc. **128**, 2115 (2006).

[14] L. R. Hirsch, R. J. Stafford, J. A. Bankson, S. R. Sershen, B. Rivera, R. E. Price, J. D. Hazle, N. J. Halas, and J. L. West, Proc. Natl. Acad. Sci. U. S. A. **100**, 13549 (2003).

[15] X. Xia, S. Xie, M. Liu, H.-C. Peng, N. Lu, J. Wang, M. J. Kim, and Y. Xia, Proc. Natl. Acad. Sci. U. S. A. **110**, 6669 (2013).

[16] Y. Lu, J. Y. Huang, C. Wang, S. Sun, and J. Lou, Nat. Nanotechnol. **5**, 218 (2010).

[17] S. Y. Kim, I.-H. Lee, and S. Jun, Phys. Rev. B **76**, 245407 (2007).

[18] S. H. Tolbert and A. P. Alivisatos, Science **265**, 373 (1994).

[19] C. L. Choi, K. J. Koski, S. Sivasankar, and A. P. Alivisatos, Nano Lett. **9**, 3544 (2009).

[20] Q. F. Gu, G. Krauss, W. Steurer, F. Gramm, and A. Cervellino,

Phys. Rev. Lett. **100**, 45502 (2008).

[21] Y. Bao, B. Zhao, D. Hou, J. Liu, F. Wang, X. Wang, and T. Cui, J. Appl. Phys. **115**, 223503 (2014).

[22] Y. Bao, B. Zhao, X. Tang, D. Hou, J. Cai, S. Tang, J. Liu, F. Wang, and T. Cui, Appl. Phys. Lett. **107**, 201909 (2015).

[23] A. Lay, D. S. Wang, M. D. Wisser, R. D. Mehlenbacher, Y. Lin, M. B. Goodman, W. L. Mao, and J. A. Dionne, Nano Lett. **17**, 4172 (2017).

[24] K. Lance Kelly, Eduardo Coronado, A. Lin Lin Zhao, and G. C. Schatz*, (2002).

[25] S. Link and M. A. El-Sayed, J. Phys. Chem. B **103**, 8410 (1999).

[26] G. V Hartland, Chem. Rev. **111**, 3858 (2011).

[27] N. Goubet, C. Yan, D. Polli, H. Portalès, I. Arfaoui, G. Cerullo, and M.-P. Pileni, Nano Lett. **13**, 504 (2013).

[28] Tanvi, A. Mahajan, R. K. Bedi, S. Kumar, V. Saxena, and D. K. Aswal, J. Appl. Phys. **117**, 83111 (2015).

[29] S. Peng, Y. Lee, C. Wang, H. Yin, S. Dai, and S. Sun, Nano Res. **1**, 229 (2008).

[30] C. . Herbst, R. . Cook, and H. . King, J. Non. Cryst. Solids **172–174**, 265 (1994).

[31] T. S. Duffy, G. Shen, D. L. Heinz, J. Shu, Y. Ma, H.-K. Mao, R. J. Hemley, and A. K. Singh, Phys. Rev. B **60**, 15063 (1999).

[32] A. K. Singh, H.-P. Liermann, Y. Akahama, S. K. Saxena, and E.

Menéndez-Proupin, J. Appl. Phys. **103**, 63524 (2008).

[33] A. K. Singh, H. P. Liermann, S. K. Saxena, H. K. Mao, and S. U. Devi, J. Phys. Condens. Matter **18**, S969 (2006).

[34] C. B. Murray, C. R. Kagan, and M. G. Bawendi, Annu. Rev. Mater. Sci. **30**, 545 (2000).

[35] M. P. Pileni, J. Phys. Chem. B **105**, 3358 (2001).

[36] Francois Cardarelli, *Materials Handbook* (Springer London, London, 2008).

[37] X. Qian and H. S. Park, J. Mech. Phys. Solids **58**, 330 (2010).

[38] C. Voisin, D. Christofilos, P. A. Loukakos, N. Del Fatti, F. Vallée, J. Lermé, M. Gaudry, E. Cottancin, M. Pellarin, and M. Broyer, Phys. Rev. B **69**, 195416 (2004).

[39] E. Hao, S. Li, R. C. Bailey, S. Zou, G. C. Schatz, and J. T. Hupp, J. Phys. Chem. B **108**, 1224 (2004).

[40] X. Ben, P. Cao, and H. S. Park, J. Phys. Chem. C **117**, 13738 (2013).

[41] D. I. Yakubovsky, A. V. Arsenin, Y. V. Stebunov, D. Y. Fedyanin, and V. S. Volkov, Opt. Express **25**, 25574 (2017).

[42] R. J. Hemley, H. Mao, G. Shen, J. Badro, P. Gillet, M. Hanfland, and D. Häusermann, Science (80-.). **276**, 1242 (1997).

[43] C. L. Choi, K. J. Koski, A. C. K. Olson, and A. P. Alivisatos, Proc. Natl. Acad. Sci. U. S. A. **107**, 21306 (2010).

[44] A. Stevenson, A. Jones, and S. Raghavan, Nano Lett. **11**, 3274

(2011).

[45] X. Jin, M. Götz, S. Wille, Y. K. Mishra, R. Adelung, and C. Zollfrank, Adv. Mater. **25**, 1342 (2013).

Figures

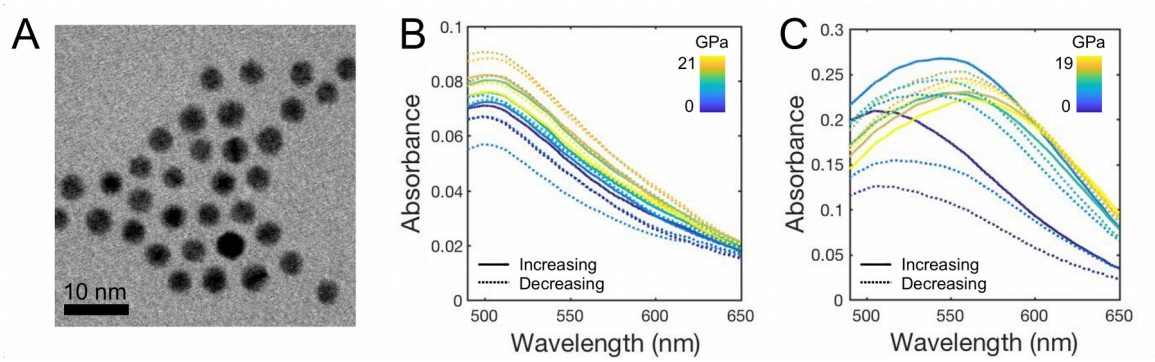

Figure 1. High-pressure optical absorbance of 3.9 nm Au nanocrystals. A) Transmission electron microscope image of nanocrystals. B) Absorbance spectra in hydrostatic pressure medium (ethylcyclohexane). C) Absorbance spectra in non-hydrostatic pressure medium (toluene). Spectra obtained during increasing pressure (loading of diamond anvil cell) are shown as a solid line. Spectra obtained during decreasing pressure (unloading of diamond anvil cell) are shown as dotted lines.

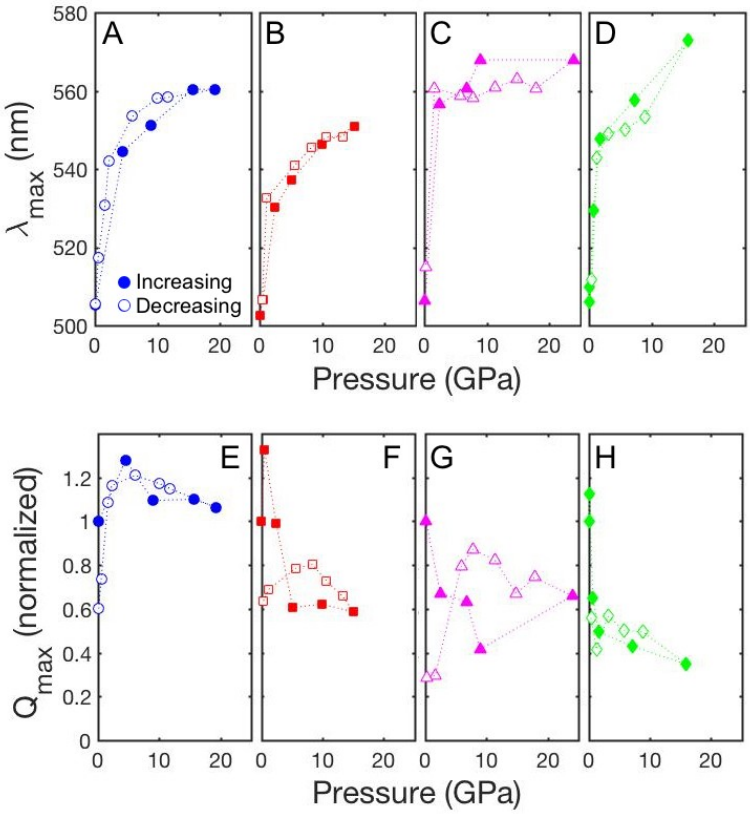

Figure 2. Plasmon peak shifts in a non-hydrostatic pressure environment. A-D) The plasmon peak wavelength (λ_{max}) and E-H) the corresponding absorbance efficiency (Q_{max}) for four independent experiments. Q_{max} is normalized to Q_{max} at ambient pressure. Measurements made during increasing pressure are shown as filled symbols. Measurements made during decreasing pressure are shown as open symbols.

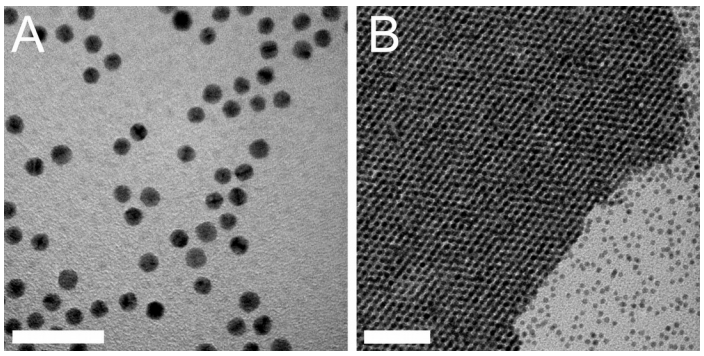

Figure 3. Transmission electron microscope images of A) individual and B) self-assembled superlattice of Au nanocrystals after compression to 30 GPa and return to atmospheric pressure (non-hydrostatic). Scale bar represents 20 nm in (A). Scale bar represents 50 nm in (B).

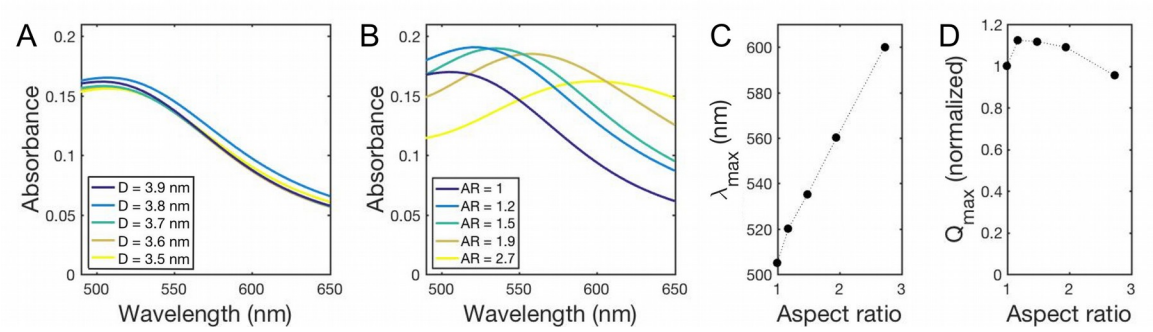

Figure 4. Simulated optical absorbance of Au nanocrystals. A) Absorbance of spherical nanocrystals with varying diameter (D). B) Absorbance of ellipsoidal spheroid nanocrystal with constant volume (equal to sphere with 3.9 nm diameter) and varying aspect ratio (AR) where AR is the ratio of the major axis to minor axis of the ellipsoidal spheroid. C) Plasmon peak wavelength (λ_{max}) and D) absorbance efficiency (Q_{max}) for the ellipsoidal spheroid nanocrystal.

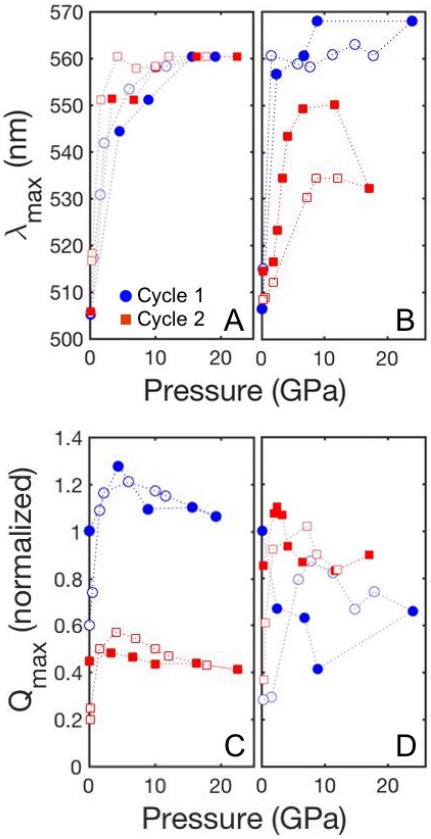

Figure 5. Plasmon peak shifts over multiple pressure cycles (non-hydrostatic). A,B) The plasmon peak wavelength (λ_{max}) and C,D) the corresponding absorbance efficiency (Q_{max}) during cycle 1 (blue) and cycle 2 (red) during two experiments. In the experiment in A, C), cycle 1 and cycle 2 are separated by a half-hour. In the experiment in B, D), cycle 1 and cycle 2 are separated by 15.5 hours (overnight). Measurements made during increasing pressure are shown as filled symbols. Measurements made during decreasing pressure are shown as open symbols.